Exact solution for 2D polygonal inclusion problem in anisotropic magnetoelectroelastic full-, half-, and bimaterial-planes

X. Jiang, E. Pan [*]

Department of Civil Engineering, University of Akron, Akron, OH 44325-3905, USA

Abstract

General inclusion problems of anisotropic and fully coupled magnetoelectroelastic solids are studied analytically in this paper. We first derive the two-dimensional Green's function in terms of the Stroh formalism in an exact closed form for magnetoelectroelastic full-, half-, and bimaterial-planes with general anisotropy. In virtue of the simple Green's function solution and the equivalent body-force concept, the elastic, electric, and magnetic fields induced by an arbitrarily shaped polygon with a uniform eigenfield inside are evaluated analytically. The solution is then applied to the nanostructures where the typical T- and V-shaped quantum wires are treated as inclusions embedded in the semiconductor substrate. While numerical results for the reduced elastic and piezoelectric cases are in consistence with previous ones, certain interesting new features on the elastic, electric, and magnetic fields are observed for the fully coupled magnetoelectroelastic solid, which could be of interest in the composite repair, and fabrication and design of novel magnetoelectroelastic semiconductor devices.
© 2004 Elsevier Ltd. All rights reserved.

Keywords: Magnetoelectroelastic Green's functions; Polygonal inclusion; Eshelby problem; Exact closed-form solution; Full-, half-, and bimaterial-planes; Quantum wire; Composite patches

1. Introduction

Many striking features have been observed as related to the coupling among the elastic, electric, and magnetic fields, such as piezoelectric (PE), piezomagnetic (PM), magnetoelectric (ME) and magnetoelectroelastic couplings (Benveniste, 1995; Erber et al., 1997; Meeker and Dozor, 1999; Sander, 1999; Aboudi, 2001; Fiebig et al., 2002; Ryu et al., 2002; Mazumder and Battacharyya, 2003). It is particularly interesting that although magnetoelectric coupling does not exist in piezoelectric or piezomagnetic phase alone, it can be acquired in the corresponding composites, and the effect could be even larger than that in some of the

---

single phase materials of magnetoelectricity (e.g., Nan, 1994). The energy conversion among elastic, electric, and magnetic forms provides numerous opportunities for potential applications of the coupling materials and structures as ultrasonic transducers, magnetic-field probes, and microdrives (Erber et al., 1997; Gibbs et al., 1997; Frank and Schilling, 1998; Meeker and Dozor, 1999; Li, 2003). In order to understand the coupling features in and among PE, PM, and ME, various analytical and numerical studies have been also carried out (Daher, 1996; Ting, 1996; Huang and Kuo, 1997; Li and Dunn, 1998; Aboudi, 2000; Li, 2000, 2003; Liu et al., 2001; Pan, 2001, 2002a; Pan and Heyliger, 2002; Chen and Lee, 2003; Ding and Jiang, 2003; Gao et al., 2003a,b; Horiguchi and Shindo, 2003; Soh et al., 2003; Wang and Zhong, 2003a,b; Pan and Han, submitted for publication).

Stimulated by potential performance improvement on semiconductor devices (Goldoni et al., 1997a, 1999), nanoscale quantum structures, namely, quantum well (QW), quantum wire (QWR) and quantum dot (QD), have been widely and intensively studied in recent years. It is noted that most semiconductor materials used in the fabrication of these nanoscale quantum structures exhibit the PE coupling, i.e., the piezoelectric coupling (Caro and Tapfer, 1995; Lomascolo et al., 1999, 2000; Andreev and O'Reilly, 2000; Liu et al., 2002; Pan, 2002b), while the PM and ME couplings are becoming current interest for researchers (Gippius et al., 1994; Miura et al., 1998; Austing et al., 1999; Mauritz et al., 2000; Lang et al., 2003). Perhaps the most attractive one is the so-called diluted magnetic semiconductor (DMS), made possible by introducing a small quantity of magnetic ion into a normal semiconductor (Dietl et al., 2001; Park et al., 2002). Associated with this novel semiconductor is the giant magnetoresistance (GMR) effect, which can be observed in layered magnetic thin-film structures consisting of a stack of alternating layers of magnetic and nonmagnetic atoms (i.e., the DMS). The corresponding ferromagnetic/semiconductor heterostructures may lead to the "marriage" of magnetic storage and semiconductor devices, and the development of next generation spin-electronics or spintronics devices for data storage and processing at the same time.

It is very interesting that under certain assumptions, the QWR induced field can be solved using the well-known Eshelby inclusion method (Ting, 1996; Mura, 1997). For the isotropic and anisotropic elastic case, various investigations on the Eshelby problems related to polygonal inclusion have been carried out (Rodin, 1996; Nozaki and Taya, 1997; Faux et al., 1997; Yu, 2001; Glas, 2003), including a very interesting application to the cracked composite repair using composite patches (Duong and Yu, 2003). For general anisotropy with PE, ME, or ME coupling, solutions to the Eshebly problems of polygonal inclusion have also been developed based on the analytical continuation and conformal mapping methods (Ru, 1999, 2000; Wang and Shen, 2003), and the Green's function method and the equivalent body-force concept (Pan and Jiang, 2003; Pan, 2004a,b). However, an exact closed-form solution for the corresponding Eshelby inclusion problem in general anisotropic and fully coupled magnetoelectroelastic solids is still lacking. Yet, such a solution could be of significant interest in future composite repairs, and fabrication and design of magnetoelectroelastic semiconductor nanostructures.

Therefore, in this paper, we derive the exact closed-form solution for the generalized Eshelby problem with an arbitrarily shaped polygonal inclusion in anisotropic magnetoelectroelastic full-, half-, and bi-material-planes. To achieve our goal, we first derive an integral expression for the induced extended displacement (defined later) in terms of the line-source Green's functions. We then derive the simple and closed-form line-source Green's functions in the full-, half-, and bimaterial-planes. Finally, we carry out the integral involved in the extended displacement expression and obtain the analytical solution. It is remarkable that even for the general anisotropic and fully coupled magnetoelectroelastic solid with arbitrarily shaped inclusions, the induced elastic, electric, and magnetic fields can be expressed in the exact closed form! The present closed-form solution is further applied to the typical T- and V-shaped QWRs and the induced field distribution inside and outside the QWR is also discussed. This paper is organized as follows: In Section 2, we describe the general inclusion problem and derive the elastic, electric, and magnetic fields in terms of the Green's functions using the equivalent body-force method (Mura, 1987; Pan, 2004a,b). The full- and half-plane Green's functions for magnetoelectroelasticity are derived in Section 3

with the corresponding bimaterial Green's functions being given in Appendix A. In Section 4, we derive the exact closed-form expressions for the induced elastic, electric, and magnetic fields inside and outside the inclusion for both the full- and half-plane cases with the corresponding results for the bimaterial-plane being given in Appendix B. While numerical studies are carried out in Section 5 for the induced fields inside and outside T- and V-shaped QWRs which reveal various interesting features, concluding remarks are made in Section 6.

2. Problem formulation

Let us assume that there is a general inclusion with arbitrary shape in anisotropic magnetoelectroelastic full- or half-plane ($z < 0$), with V denoting the inclusion and ∂V boundary of the inclusion. An extended uniform eigenstrain $\gamma_{Ij}^*(\gamma_{ij}^*, -E_j^*, -H_j^*)$ is applied inside the inclusion (Fig. 1). While the elastic eigenstrain is due to the mismatched lattice constants between the QWR and matrix (Faux et al., 1997), the eigen-electric field and eigen-magnetic field could be directly connected to the spontaneous polarization and magnetization (e.g., see Jogai et al., 2003). For the half-plane case, the surface of the half-plane ($z = 0$) is assumed to be traction-free (i.e., the elastic traction, the normal components of the electric displacement and magnetic induction are zero).

We first define the extended constitutive relationship as (Pan, 2002b):

$$\sigma_{iJ} = C_{iJKl}\gamma_{Kl} \tag{1a}$$

with

$$
\gamma_{Ij} =
\begin{cases}
\gamma_{ij}, & I = i = 1,2,3 \\
-E_j, & I = 4 \\
-H_j, & I = 5
\end{cases}
\qquad
C_{iJKl} =
\begin{cases}
C_{ijkl}, & J,\ K = j,\ k = 1,2,3 \\
e_{lij}, & J = j = 1,2,3;\ K = 4 \\
e_{ikl}, & J = 4;\ K = k = 1,2,3 \\
q_{lij}, & J = j = 1,2,3;\ K = 5 \\
q_{ikl}, & J = 5;\ K = k = 1,2,3 \\
-\lambda_{il}, & J = 4;\ K = 5;\ J = 5,\ K = 4 \\
-\varepsilon_{il}, & J = K = 4 \\
-\mu_{il}, & J = K = 5
\end{cases}
\tag{1b}
$$

$$
\sigma_{iJ} =
\begin{cases}
\sigma_{ij}, & J = j = 1,2,3 \\
D_i, & J = 4 \\
B_i, & J = 5
\end{cases}
$$

In the above equations, γ_{ij}, E_i, and H_i are the elastic strain, electric field, and magnetic field, respectively; σ_{ij}, D_i, and B_i are the elastic stress, electric displacement, and magnetic induction (i.e., magnetic flux),
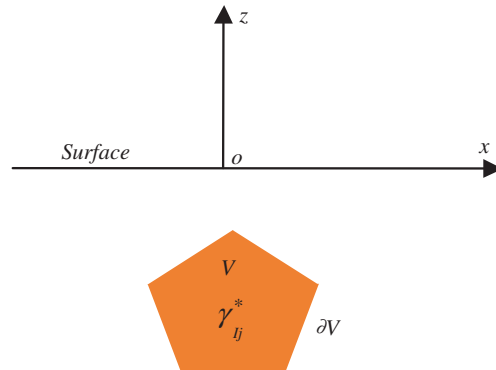

Fig. 1. A general inclusion problem in an anisotropic magnetoelectroelastic (x,z)-half-plane ($z < 0$): an extended eigenstrain $\gamma_{Ij}^*(\gamma_{ij}^*, -E_j^*, -H_j^*)$ within an arbitrarily shaped polygon.

respectively; C_{ijkl}, ε_{ij}, and μ_{ij} are the elastic, dielectric, and magnetic permeability coefficients, respectively; e_{ijk}, q_{ijk}, and λ_{ij} are the piezoelectric, piezomagnetic, and magnetoelectric coefficients, respectively. It is apparent that the fully coupled model can be reduced to various uncoupled ones by setting the appropriate coefficients to zero (Pan, 2002a).

The extended strain–displacement relation for small deformation is (Pan and Heyliger, 2002):

$$\gamma_{ij} = 0.5(u_{i,j} + u_{j,i}); \quad E_i = -\phi_{,i}; \quad H_i = -\psi_{,i} \tag{2}$$

where u_i, ϕ, and ψ are the elastic displacement, electric potential, and magnetic potential, respectively.

The equilibrium equations for the stresses, and the balance for the electric displacement and magnetic induction are

$$\sigma_{iJ,i} = 0 \tag{3}$$

Based on the method of superposition and equivalence body-force concept, and following the procedure of Pan (2004a,b), we express the extended displacement $u_K(u_k, \phi, \psi)$ at $X = (X, Z)$ as an integral over the boundary of the inclusion as

$$u_K(X) = C_{iJLm}\gamma_{Lm}^* \int_{\partial V} u_J^K(x; X)n_i(x)\,dS(x) \tag{4}$$

where $n_i(x)$ is the outward normal on the boundary ∂V; and $u_J^K(x; X)$ is the Jth Green's elastic displacement/electric potential/magnetic potential at $x = (x, z)$ due to a line-force/line-charge/line-current in the Kth direction applied at X.

3. Two-dimensional magnetoelectroelastic Green's functions

3.1. Full-plane

We take the model system consisting of an infinitely long cylinder with a polygonal cross section within a magnetoelectroelastic space. The problem can thus be reduced to a generalized 2D plane-strain deformation in (x, z) plane. In other words, the deformation is independent of y-coordinate so that we only consider field distribution on the cross section parallel to the (x, z) plane. We also assume that an extended line force $f = (f_1, f_2, f_3, -f_e, -f_m)$ is applied at (X, Z).

Extending the anisotropic piezoelectric full-plane Green's functions using Stroh formalism (Ting, 1996) to the general magnetoelectroelastic case, we find that the extended displacement vector $\boldsymbol{u}$ and stress function vector $\boldsymbol{\psi}$ have expressions:

$$\boldsymbol{u} = \frac{1}{\pi}\text{Im}\{\boldsymbol{A}\langle\ln(z_* - s_*)\rangle\boldsymbol{q}^\infty\}$$
$$\boldsymbol{\psi} = \frac{1}{\pi}\text{Im}\{\boldsymbol{B}\langle\ln(z_* - s_*)\rangle\boldsymbol{q}^\infty\} \tag{5}$$

in which Im stands for the imaginary part, and p_J (contained in z_* and s_* as shown in Eqs. (6) and (7)), $\boldsymbol{A}$, and $\boldsymbol{B}$ are the Stroh eigenvalues and corresponding eigenvectors. Also in Eq. (5) we have:

$$\langle\ln(z_* - s_*)\rangle = \text{diag}[\ln(z_1 - s_1), \ln(z_2 - s_2), \ln(z_3 - s_3), \ln(z_4 - s_4), \ln(z_5 - s_5)] \tag{6}$$

where z_J and $s_J(J = 1, 2, 3, 4, 5)$ are complex variables associated with the field and source points of the Green's functions, and are defined as

$$z_J = x + p_J z, \quad s_J = X + p_J Z \tag{7}$$

It is further noticed that in Eq. (5) we have

$$\boldsymbol{q}^{\infty} = \boldsymbol{A}^{\mathrm{T}} \boldsymbol{f} \tag{8}$$

where the superscript T denotes the matrix transpose.

3.2. Half-plane

The Green's functions for anisotropic magnetoelectroelastic half plane can be obtained following the work of Ting (1996) and Pan (2004a,b). In other words, the extended displacement vector $\boldsymbol{u}$ and stress function vector $\boldsymbol{\psi}$ assume the following forms:

$$
\begin{aligned}
\boldsymbol{u} &= \frac{1}{\pi}\mathrm{Im}\{\boldsymbol{A}\langle\ln(z_* - s_*)\rangle\boldsymbol{q}^{\infty}\} + \frac{1}{\pi}\mathrm{Im}\sum_{J=1}^{5}\left\{\boldsymbol{A}\langle\ln(z_* - \bar{s}_J)\rangle\boldsymbol{q}_J\right\} \\
\boldsymbol{\psi} &= \frac{1}{\pi}\mathrm{Im}\{\boldsymbol{B}\langle\ln(z_* - s_*)\rangle\boldsymbol{q}^{\infty}\} + \frac{1}{\pi}\mathrm{Im}\sum_{J=1}^{5}\left\{\boldsymbol{B}\langle\ln(z_* - \bar{s}_J)\rangle\boldsymbol{q}_J\right\}
\end{aligned}
\tag{9}
$$

where

$$\langle\ln(z_* - \bar{s}_J)\rangle = \mathrm{diag}[\ln(z_1 - \bar{s}_J), \ln(z_2 - \bar{s}_J), \ln(z_3 - \bar{s}_J), \ln(z_4 - \bar{s}_J), \ln(z_5 - \bar{s}_J)], \tag{10a}$$

an over-bar indicates complex conjugate, and $\boldsymbol{q}_J$ is defined as

$$\boldsymbol{q}_J = \boldsymbol{K}^{-1}\bar{\boldsymbol{K}}\boldsymbol{I}_J\bar{\boldsymbol{q}}^{\infty} \tag{10b}$$

with the matrix $\boldsymbol{K}$ taking care of the boundary conditions on the surface of the half plane (Pan, 2004a,b; see also Eq. (15) below), and diagonal matrices $\boldsymbol{I}_J$ having the form:

$$
\begin{aligned}
&\boldsymbol{I}_1 = \mathrm{diag}[1,0,0,0,0]; \quad \boldsymbol{I}_2 = \mathrm{diag}[0,1,0,0,0]; \quad \boldsymbol{I}_3 = \mathrm{diag}[0,0,1,0,0]; \\
&\boldsymbol{I}_4 = \mathrm{diag}[0,0,0,1,0]; \quad \boldsymbol{I}_5 = \mathrm{diag}[0,0,0,0,1]
\end{aligned}
\tag{11}
$$

We point out that the first term in Eq. (9) corresponds to the full-plane Green's functions while the second term is the complementary part resulting from the effect of the free surface of the half plane. We further mention that the 2D magnetoelectroelastic Green's functions for the corresponding bimaterials can also be derived similarly and the results are given in Appendix A for the sake of completeness. With these Green's functions, Eq. (4) can be evaluated to get the extended displacements. However, we will prove in the next section that after substitution of the Green's functions into Eq. (4), the integral involved can be evaluated analytically and the resulting solution has a very simple and exact closed form.

4. Analytical solution

Substituting the Green's functions in Eqs. (5) and (9) into Eq. (4) and integrating with respect to the field point (of the Green's function) over each line segment forming the boundary of the polygon, we achieve the exact closed-form solution for the inside and outside elastic, electric, and magnetic fields in both full- and half-planes.

Let us set a generic line segment along the boundary of the inclusion from point 1 (x_1, z_1) to point 2 (x_2, z_2) as the sth line segment, with length $l^{(s)} = \sqrt{(x_2 - x_1)^2 + (z_2 - z_1)^2}$. Then we carry out the integration of the right-hand side of Eq. (4) from point 1 to point 2, sum over all the line segments, and find the following exact closed-form expression for the extended displacement in the magnetoelectroelastic half-plane:

$$u_K(\boldsymbol{X}) = \sum_{s=1}^{N} n_i^{(s)} C_{iJLm} \gamma_{Lm}^* \frac{l^{(s)}}{\pi} \operatorname{Im}\left\{ A_{JR} h_R^{(s)}(X,Z) A_{KR} + \sum_{v=1}^{5} A_{JR} g_{Rv}^{(s)}(X,Z) Q_{RK}^v \right\} \tag{12}$$

where $n_i^{(s)}$ is the ith outward normal component of the sth line segment given by

$$n_1^{(s)} = (z_2 - z_1)/l^{(s)}; \quad n_3^{(s)} = -(x_2 - x_1)/l^{(s)} \tag{13}$$

Also in Eq. (12), matrix $\boldsymbol{Q}$ is defined as

$$Q_{RN}^v = K_{RS}^{-1} \bar{K}_{Sv} \bar{A}_{Nv} \tag{14}$$

with the superscript "-1" denoting inverse matrix, and the matrix $\boldsymbol{K}$ having the form as

$$\boldsymbol{K} = \boldsymbol{I}_u \boldsymbol{A} + \boldsymbol{I}_t \boldsymbol{B} \tag{15}$$

where $\boldsymbol{I}_u$ and $\boldsymbol{I}_t$ are 5×5 diagonal matrices whose five diagonal elements are either one or zero, and satisfy conditions:

$$\boldsymbol{I}_u + \boldsymbol{I}_t = \boldsymbol{I}; \quad \boldsymbol{I}_u \boldsymbol{I}_t = 0 \tag{16}$$

with $\boldsymbol{I}$ being an identity matrix of 5×5.

We also point out that, the first term containing $h_R^{(s)}$ in Eq. (12) stands for the contribution from the full-plane Green's functions, and the one involving $g_{Rv}^{(s)}$ for the contribution from the boundary condition on the surface of the half plane. $h_R^{(s)}$ and $g_{Rv}^{(s)}$ can be expressed, respectively, as

$$h_R^{(s)}(X,Z) = \int_0^1 \ln\{[(x_2 - x_1) + p_R(z_2 - z_1)]t + [(x_1 + p_R z_1) - s_R]\}\, \mathrm{d}t$$

$$g_{Rv}^{(s)}(X,Z) = \int_0^1 \ln\{[(x_2 - x_1) + p_R(z_2 - z_1)]t + [(x_1 + p_R z_1) - \overline{s_v}]\}\, \mathrm{d}t \tag{17}$$

and after integration eventually have explicit expressions as

$$h_R^{(s)}(X,Z) = \frac{(x_1 + p_R z_1) - s_R}{(x_2 - x_1) + p_R(z_2 - z_1)} \ln\left[\frac{x_2 + p_R z_2 - s_R}{x_1 + p_R z_1 - s_R}\right] + \ln[x_2 + p_R z_2 - s_R] - 1$$

$$g_{Rv}^{(s)}(X,Z) = \frac{(x_1 + p_R z_1) - \bar{s}_v}{(x_2 - x_1) + p_R(z_2 - z_1)} \ln\left[\frac{x_2 + p_R z_2 - \bar{s}_v}{x_1 + p_R z_1 - \bar{s}_v}\right] + \ln[x_2 + p_R z_2 - \bar{s}_v] - 1 \tag{18}$$

Implementing the basic elastic strain–displacement, electric field-electric potential and magnetic field-magnetic flux relations (Pan, 2004a,b), the induced elastic strain, electric and magnetic fields can also be obtained in the exact closed form ($\alpha, \beta = 1, 3$):

$$\gamma_{\beta\alpha}(\boldsymbol{X}) = \sum_{s=1}^{N} 0.5 n_i^{(s)} C_{iJLm} \gamma_{Lm}^* \frac{l_i^{(s)}}{\pi} \operatorname{Im}\left\{ A_{JR} h_{R,\alpha}^{(s)}(X,Z) A_{\beta R} + \sum_{v=1}^{5} A_{JR} g_{Rv,\alpha}^{(s)}(X,Z) Q_{R\beta}^v \right\}$$

$$+ \sum_{s=1}^{N} 0.5 n_i^{(s)} C_{iJLm} \gamma_{Lm}^* \frac{l_i^{(s)}}{\pi} \operatorname{Im}\left\{ A_{JR} h_{R,\beta}^{(s)}(X,Z) A_{\alpha R} + \sum_{v=1}^{5} A_{JR} g_{Rv,\beta}^{(s)}(X,Z) Q_{R\alpha}^v \right\} \tag{19a}$$

$$\gamma_{2\alpha}(\boldsymbol{X}) = \sum_{s=1}^{N} 0.5 n_i^{(s)} C_{iJLm} \gamma_{Lm}^* \frac{l_i^{(s)}}{\pi} \operatorname{Im}\left\{ A_{JR} h_{R,\alpha}^{(s)}(X,Z) A_{2R} + \sum_{v=1}^{5} A_{JR} g_{Rv,\alpha}^{(s)}(X,Z) Q_{R2}^v \right\} \tag{19b}$$

$$E_\alpha(\boldsymbol{X}) = -\sum_{s=1}^{N} n_i^{(s)} C_{iJLm} \gamma_{Lm}^* \frac{l_i^{(s)}}{\pi} \mathrm{Im} \left\{ A_{JR} h_{R,\alpha}^{(s)}(X,Z) A_{4R} + \sum_{v=1}^{5} A_{JR} g_{Rv,\alpha}^{(s)}(X,Z) Q_{R4}^v \right\} \tag{19c}$$

$$H_\alpha(\boldsymbol{X}) = -\sum_{s=1}^{N} n_i^{(s)} C_{iJLm} \gamma_{Lm}^* \frac{l_i^{(s)}}{\pi} \mathrm{Im} \left\{ A_{JR} h_{R,\alpha}^{(s)}(X,Z) A_{5R} + \sum_{v=1}^{5} A_{JR} g_{Rv,\alpha}^{(s)}(X,Z) Q_{R5}^v \right\} \tag{19d}$$

Thus, we have derived the exact closed-form solutions of the extended displacement, strain, and stress fields due to a straight-line segment on the boundary of the inclusion. If all or part of the boundary is curved, one can use line-segments of small length to approximate the curved line. We also remark that the above solutions are for the induced fields in the anisotropic magnetoelectroelastic half-plane; for the corresponding full-plane case, we need to extract only those terms containing $h_R^{(s)}$ or its derivative from the above solutions. Furthermore, the corresponding solutions in bimaterials are also provided in Appendix B.

5. Numerical studies

To test the accuracy and generality of the inclusion solution derived in this paper, we first examine the cases in Pan and Jiang (2003) and Pan (2004a,b) where we studied the elastic and electric field distributions in GaAs substrate containing QWR inclusion with certain shapes. The decoupled piezoelectric solutions are obtained from the general magnetoelectroelectric coupled solution presented in this paper by setting the piezomagnetic (q_{ijk}) and electromagnetic (λ_{ij}) coefficients to be zero. It is found that the results based on the formulation given in this paper agree with those in previous research work (Pan and Jiang, 2003; Pan, 2004a,b).

Another check for our solutions is the well-known benchmark result, that is, the induced fields inside an elliptical inclusion of a uniform eigenstrain in a full plane are uniform (i.e., Eshelby, 1957; Ru, 2000). In this test, the eigenstrain inside the inclusion is assumed to be $\gamma_{xx}^* = \gamma_{yy}^* = \gamma_{zz}^* = 1$ and the material properties selected for this and the following cases are listed in Table 1 (Pan, 2002a). It is noted that these properties are chosen from the composite materials consisting of fiber reinforcement which is piezoelectric $BaTiO_3$ and matrix which is magnetostrictive $CoFe_2O_4$. For an elliptical inclusion in the anisotropic magnetoelectroelastic full plane, we let the center of ellipse be at $O(0,0)$ with its major axis equal to 20 nm and minor axis 10 nm. A polygon with N sides is employed to approximate the inclusion.

Table 2 demonstrates the strain component γ_{xx} at different locations (X,Z) $(X=Z)$ within the polygonal inclusion when the polygon has sides $N = 25, 50, 100, 500,$ and 1000. We observe clearly from Table 2 that as N increases, in other words, as the polygon approaches an ellipse, the strain component γ_{xx} becomes uniform within the ellipse. Table 3 presents the strain component γ_{zz}, electric field components E_x, E_z and magnetic components H_x, H_z when $N = 500$, with E_x and H_x being zeros due to the transverse isotropy of the material. The result in Table 3 again verifies our exact closed-form solution.

Table 1
Material properties of the fully coupled magnetoelectroelastic solid (C_{ij} in 10^9 N/m^2, e_{ij} in C/m^2, λ_{ij} in N s/V C, ε_{ij} in 10^{-9} C/V m, μ_{ij} in 10^{-6} N s^2/C^2, and q_{ij} in N/A m)

$C_{11} = C_{22}$	C_{12}	$C_{13} = C_{23}$	C_{33}	$C_{44} = C_{55}$	$C_{66} = 0.5(C_{11}-C_{12})$
166	77	78	162	43	44.5
$e_{31} = e_{32}$	e_{33}	$e_{24} = e_{15}$	$q_{31} = q_{32}$	q_{33}	$q_{15} = q_{24}$
−4.4	18.6	11.6	580.3	699.7	550
$\varepsilon_{11} = \varepsilon_{22}$	ε_{33}	$\mu_{11} = \mu_{22}$	μ_{33}		$\lambda_{ij}(i,j = 1–3)$
11.2	12.6	5	10		0

Table 2
Horizontal strain component γ_{xx} at (X, Z) $(X = Z)$ within the inclusion of N-sided regular polygon with $N = 25, 50, 100, 500,$ and 1000

$X = Z$ (nm)	$N = 25$	$N = 50$	$N = 100$	$N = 500$	$N = 1000$
0	0.680751	0.680751	0.680746	0.680746	0.680747
1	0.680743	0.680751	0.680746	0.680746	0.680747
2	0.680741	0.680751	0.680746	0.680746	0.680747
3	0.680773	0.680751	0.680746	0.680746	0.680747
4	0.680808	0.680752	0.680747	0.680746	0.680747
5	0.680829	0.680754	0.680747	0.680747	0.680747
6	0.681212	0.680738	0.680748	0.680747	0.680747
7	0.681391	0.680712	0.680749	0.680748	0.680747
8	0.673576	0.681110	0.680758	0.680752	0.680748

Table 3
Elastic, electric ($\times 10^7$ V/m), and magnetic ($\times 10^7$ A/m) fields at (X, Z) $(X = Z)$ within the inclusion of a 500-sided regular polygon

X, Z (nm)	γ_{zz}	E_x	E_z	H_x	H_z
0	1.18106	0.0000	−129.070	0.00000	1.56973
1	1.18106	0.0000	−129.070	0.00000	1.56973
2	1.18106	0.0000	−129.070	0.00000	1.56973
3	1.18106	0.0001	−129.070	0.00000	1.56973
4	1.18106	0.0002	−129.070	0.00000	1.56973
5	1.18106	0.0003	−129.070	0.00000	1.56973
6	1.18106	0.0005	−129.070	0.00000	1.56973
7	1.18106	0.0005	−129.070	0.00001	1.56972
8	1.18106	0.0005	−129.070	0.00001	1.56970

After testing our solutions, we now apply the exact closed-form solutions to the QWRs with T-shaped and crescent-shaped (V-shaped, or V-grooved) cross section, embedded in either the full- or half-plane substrate. Fig. 2 shows the geometry of a T-shaped QWR in the magnetoelectroelastic full-plane, obtained from experimental observations of Goldoni et al. (1997b), Rossi et al. (1997, 1999), Grundmann et al. (1998), and Itoh et al. (2003). The T-shaped QWR is formed by intersecting two QW structures where the carrier is confined only in one direction.

Figs. 3–6 show the field distribution within the region bounded by the dashed rectangle *PQRS* in Fig. 2. It is evident that corner/vertex points cause concentration, and that the distribution of elastic, electric, and
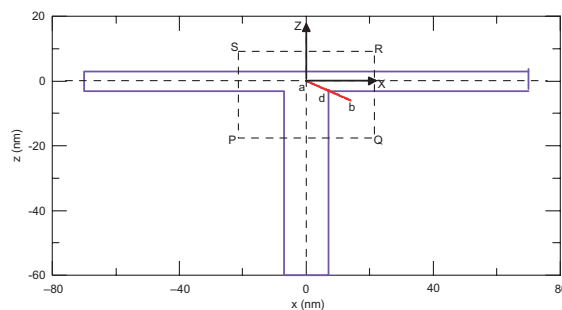

Fig. 2. A T-shaped QWR within the full-plane substrate. While the dashed rectangle *PQRS* is the region shown in Figs. 3–5, the line *ab* indicates where the singular behavior is tracked as shown in Fig. 6.
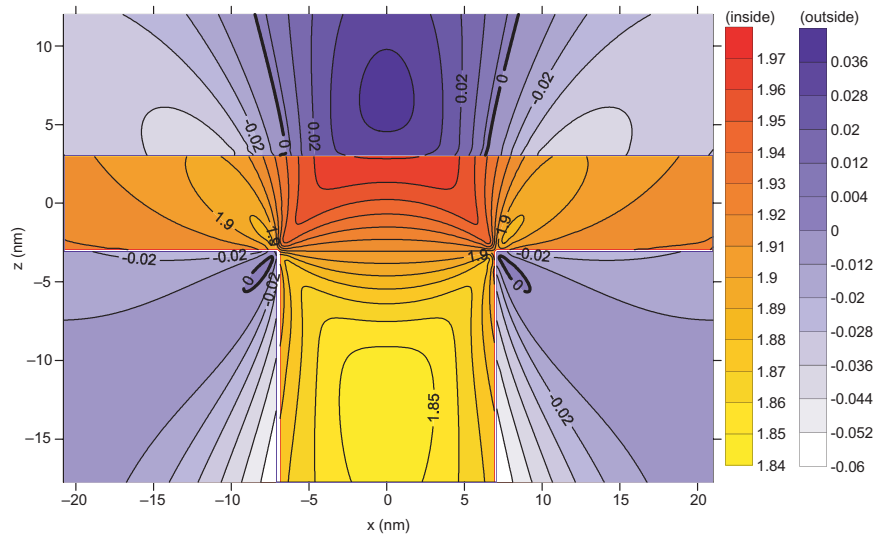
Fig. 3. Hydrostatic strain $\gamma_{xx} + \gamma_{zz}$ distribution inside and outside the T-shaped QWR in the full-plane magnetoelectroelastic substrate.
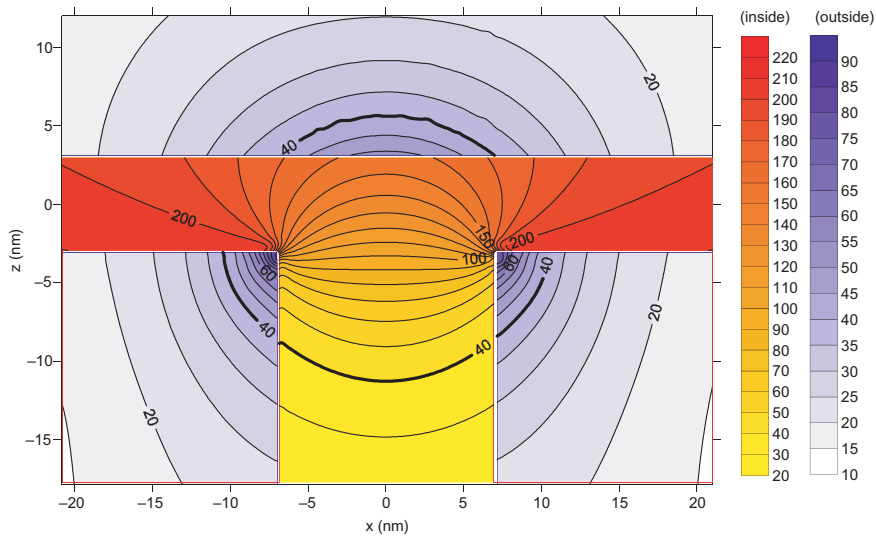

Fig. 4. Total electric field $\sqrt{E_x^2 + E_z^2}$ ($\times 10^7$ V/m) distribution inside and outside the T-shaped QWR in the full-plane magnetoelectroelastic substrate.

magnetic fields are all symmetric with respect to the *z*-axis due to the fact that both the geometry and material property are symmetric.

Firstly, contours of hydrostatic strain distribution are plotted in Fig. 3. It is clear that the strain distribution is strongly influenced by the QWR cross-section shape, particularly by the location of the vertex or corner point of the QWR. We also observe that the inside field is larger than the outside field, being as high as twice the uniform eigenstrain within the inclusion. The thick line denotes zero hydrostatic strain separating the tensile (>0) region from the compressive (<0) one. The maximum hydrostatic strain occurs at
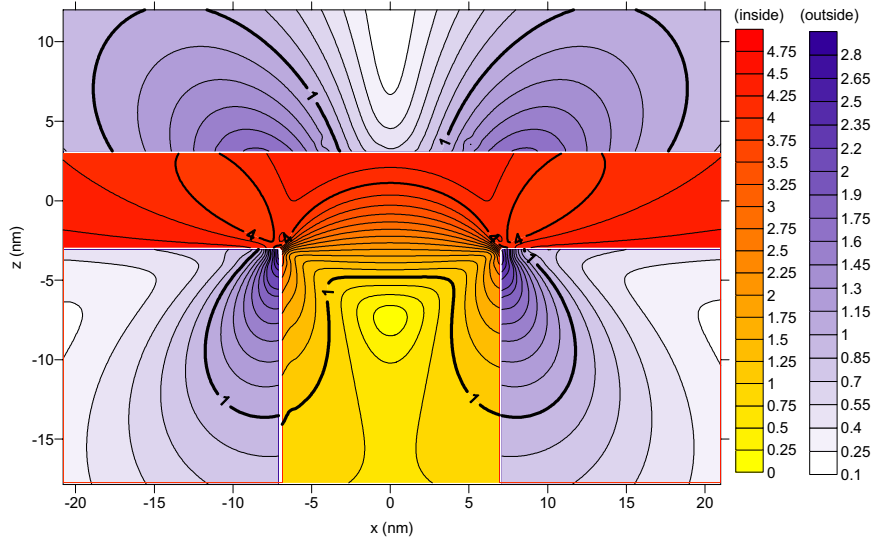
Fig. 5. Total magnetic field $\sqrt{H_x^2 + H_z^2}$ ($\times 10^7$A/m) distribution inside and outside the T-shaped QWR in the full-plane magnetoelectroelastic substrate.
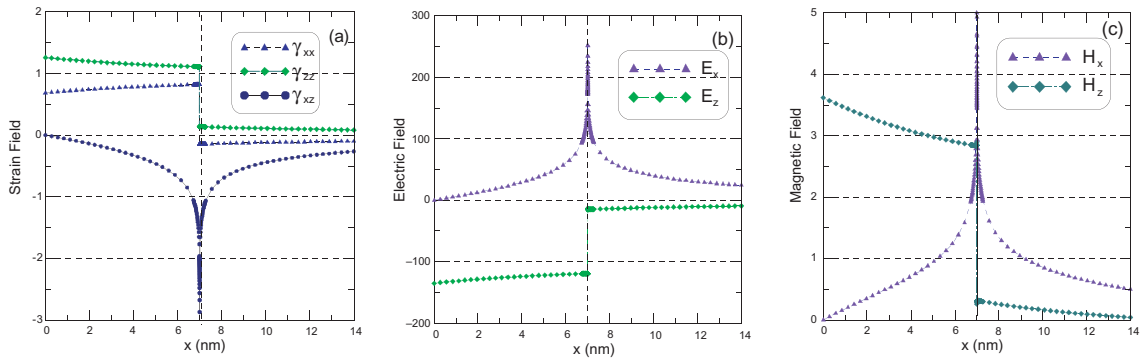

Fig. 6. Strain components γ_{xx}, γ_{zz}, and γ_{xz} in (a), electric fields E_x and E_z ($\times 10^7$ V/m) in (b), and magnetic fields H_x and H_z ($\times 10^7$ A/m) in (c), along the line ab (i.e., $x = -3z/7$) shown in Fig. 2 with the middle being at the corner point d (7, −3 nm).

the center of the top part of T-shape (Fig. 3). Secondly, Fig. 4 shows the total electric field. The most interesting feature associated with the electric field is that in the lower part of region, the electric fields inside and outside the T-shaped QWR are continuous across the two vertical boundary lines of the QWR (see, e.g., the thick contour line representing 40×10^7 V/m). Thirdly, Fig. 5 shows the corresponding total magnetic field. Similarly, the magnetic fields inside and outside the T-shaped QWR are continuous across the two vertical boundary lines of the QWR (e.g., the thick contour line representing 1×10^7 A/m). Finally, Fig. 6a, b, and c show the variation of the strain, electric, and magnetic fields along the line ab with its middle at corner point d (7 nm, −3 nm) as indicated in Fig. 2. Observation of these figures reveals that while the strain components γ_{xx} and γ_{zz} are finite at this corner, the strain component γ_{xz} shows a logarithmic singularity (Fig. 6a). As for the electric and magnetic fields, the horizontal electric component E_x (Fig. 6b) and magnetic component H_x (Fig. 6c) are singular at the corner whilst their corresponding vertical com-

ponents are finite. This feature has never been reported in any literature, and could be helpful in the future composite repair, and fabrication and design of magnetoelectroelastic QWR structures.

We then apply our solution to the same T-shaped QWR but in the magnetoelectroelastic half-plane substrate (Fig. 7), with results shown in Figs. 8–10. Comparing the induced fields in the half-plane to those in the full-plane substrate, i.e., Fig. 8 vs. Fig. 3; Fig. 9 vs. Fig. 4; Fig. 10 vs. Fig. 5, one can clearly observe the influence of the free surface of the half-plane on the induced fields. In general, the outside fields on top of the T-shaped QWR are affected mostly. For instance, while the magnitude of the inside hydrostatic strain (Fig. 8) increases to about 2.2 for the half-plane case, instead of 2.0 for the full-plane case (Fig. 3), the outside hydrostatic strain above the T-shaped QWR increases to 0.35 at the center of the free surface, almost seven times larger than that for corresponding full-plane case. Furthermore, all the outside hydrostatic strain becomes positive for the half-plane case (Fig. 8 vs. Fig. 3). It is also interesting that the
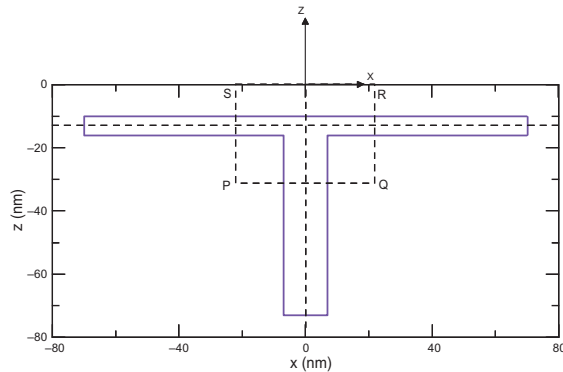

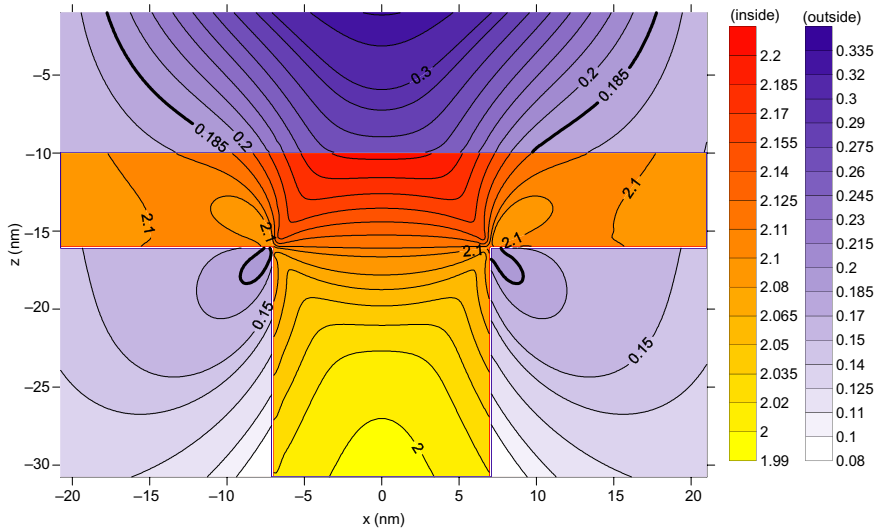Fig. 7. A T-shaped QWR within a half-plane substrate ($z < 0$).

Fig. 8. Hydrostatic strain $\gamma_{xx} + \gamma_{zz}$ distribution inside and outside the T-shaped QWR in the half-plane magnetoelectroelastic substrate ($z < 0$).
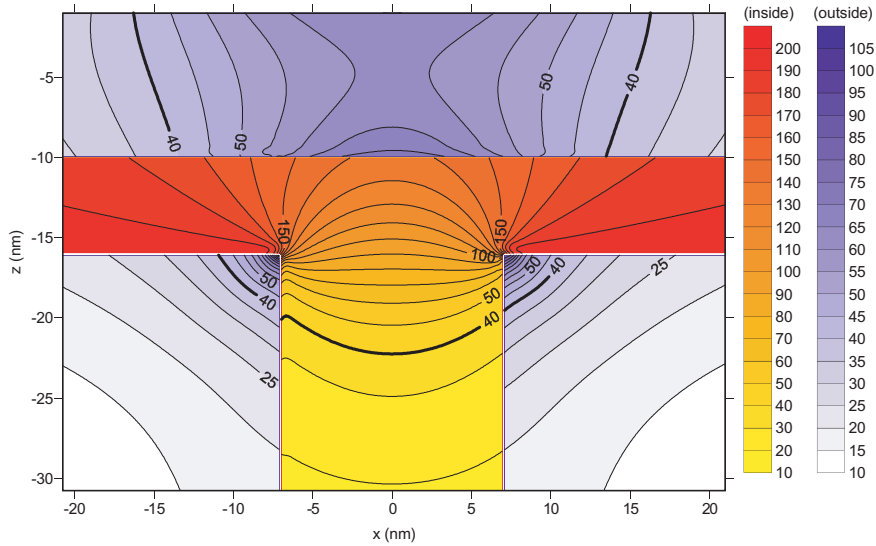
Fig. 9. Total electric field $\sqrt{E_x^2 + E_z^2}$ ($\times 10^7$ V/m) distribution inside and outside the T-shaped QWR in the half-plane magnetoelectroelastic substrate ($z < 0$).
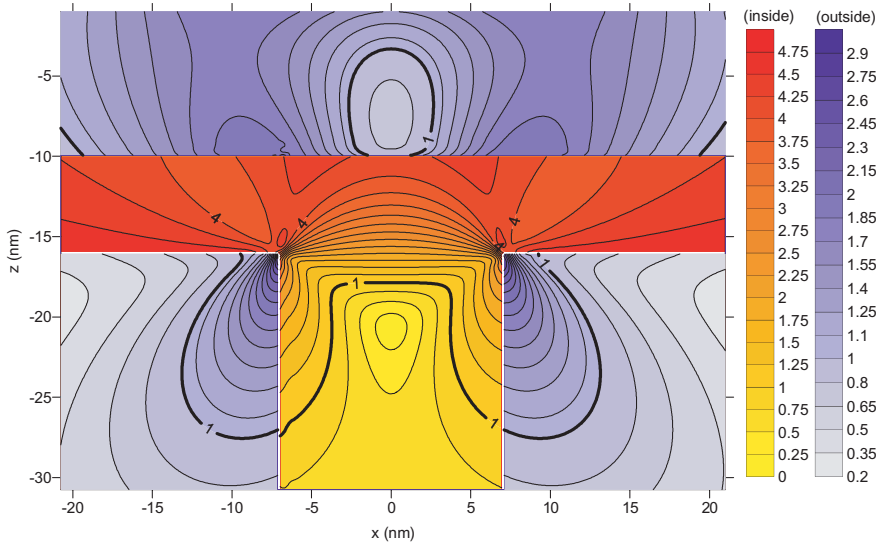

Fig. 10. Total magnetic field $\sqrt{H_x^2 + H_z^2}$ ($\times 10^7$ A/m) distribution inside and outside the T-shaped QWR in the half-plane magneto-electroelastic substrate ($z < 0$).

free surface has only slight influence on both the electric and magnetic fields, and the most affected area is on top of the T-shaped QWR (Figs. 9 and 10), where one can also see the change of contour shapes due to the existence of the free surface (Fig. 9 vs. Fig. 4; Fig. 10 vs. Fig. 5). However, the lower part of the inside and outside regions does not experience much changes, and in particular, the fields inside and outside are

still continuous across the two vertical lines of the QWR boundary (Figs. 9 and 10). Therefore, in the fabrication and design of QWR structure, the distance of the QWR to the free surface needs to be carefully arranged and the features we observed also need to be taken into consideration.

Finally, we study the 'classic' V-shaped QWR structure (Kapon et al., 1989; Rinaldi et al., 1994; Gustafsson et al., 1994, 1996; Grundmann et al., 1994; Goldoni et al., 1996; Rossi et al., 1997, 1999) in the semiconductor full-plane using our solutions. The V-shaped QWR has a crescent cross section (Fig. 11) where the upper boundary of the crescent is part of the circle with radius of 26.66 nm, and the lower part is formed by two straight-line segments BI and CJ and part of a circle with radius of 13 nm. The two straight-line segments are at an angle of 54.74° from the horizontal x-axis and the maximum thickness of the crescent, OA, equals 10 nm (Kapon et al., 1992; Faux et al., 1997). The mechanism involved in the formation of crescent-shaped QWR during fabrication is discussed in Kapon et al. (1992).

Similar to the T-shaped QWR, the V-shaped QWR is symmetric with respect to the z-axis and thus the induced fields are also symmetric (Figs. 12–14). It is noted that the induced response inside is much larger than that outside, with the exception of the magnetic field where both inside and outside fields have the same magnitude (Fig. 14). Again, with the exception of the magnetic field, the contours of the elastic strain and electric fields inside the QWR seem to follow the shape of the crescent curve, as demonstrated in Figs. 12 and 13. Furthermore, the electric field outside also follows the shape of the crescent curve (Fig. 13) while the strain and magnetic fields outside show concentrations at different locations (Figs. 12 and 14). It is interesting to point out that as far as the elastic strain field (Fig. 12) is concerned, the contour lines of zero value, which extend from the tips of the QWR, are almost coincide with the two lines-segments BI and CJ that bound the V shape (in particular for γ_{xx} and γ_{zz} in Fig. 12 a and b, respectively).

In summary, for the T-shaped QWR within the substrate, the following features are observed:

(1) The shear strain component, horizontal electric and magnetic fields are singular at the corners of the QWR, whilst other components are finite there. The singular behavior of electric and magnetic fields has not been discussed before in any literature;
(2) The induced response inside the QWR is usually larger than that outside;
(3) In the lower part of the T-shaped QWR structure, the electric and magnetic fields are continuous across the two vertical lines of the QWR boundary, whilst the strain field is still discontinuous;
(4) Free surface of the QWR structure can have a strong influence on the induced field, in particular, in the upper part of the QWR.
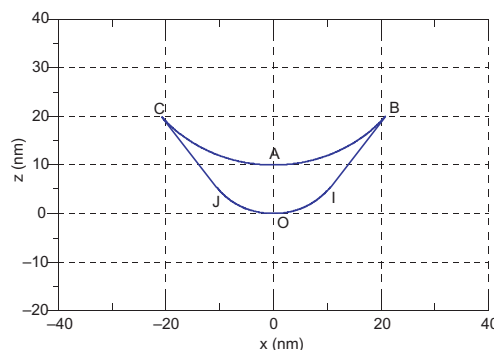

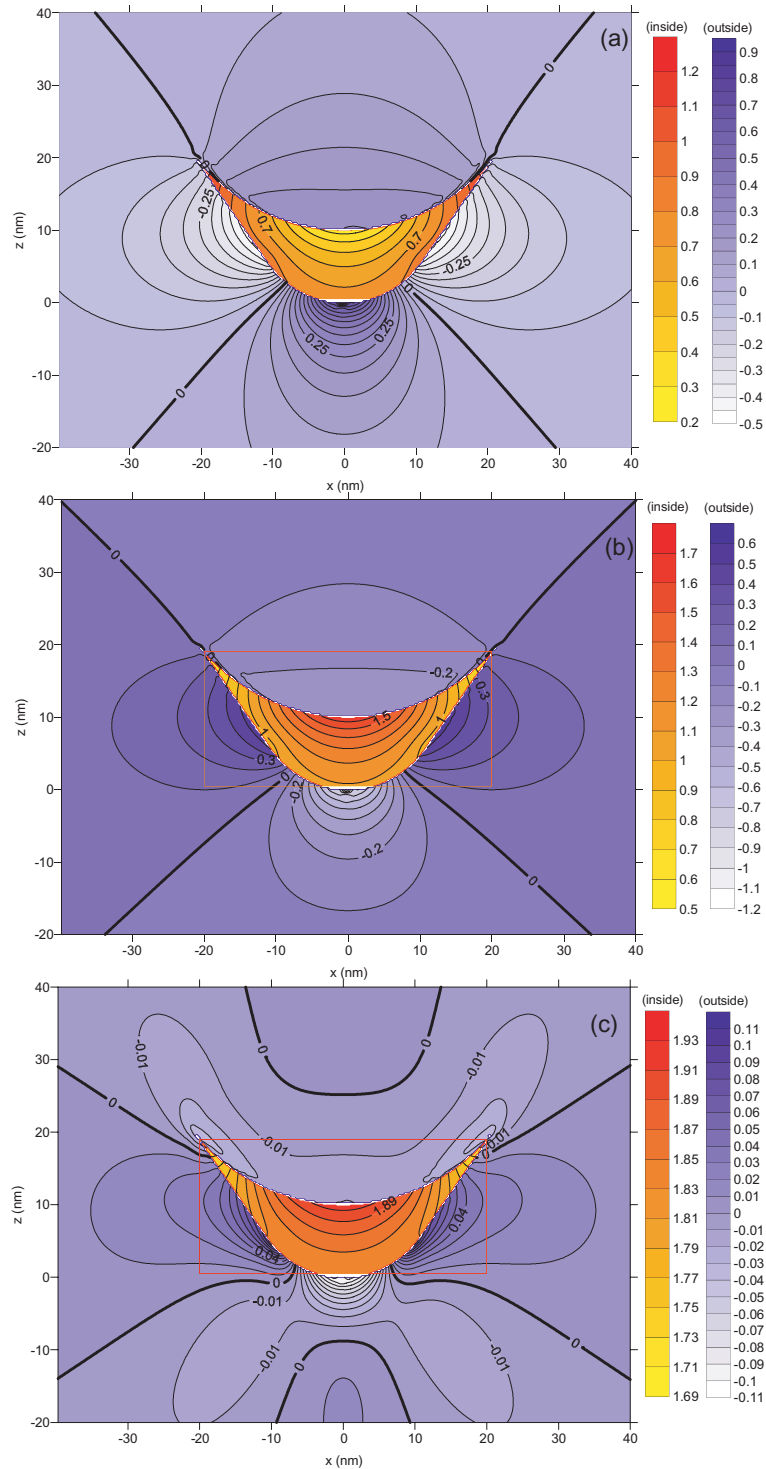Fig. 11. A crescent/V-shaped QWR within the full-plane substrate.

Fig. 12. Distributions of strain component γ_{xx} in (a), γ_{zz} in (b), and hydrostatic strain $\gamma_{xx} + \gamma_{zz}$ in (c), inside and outside the crescent/V-shaped QWR in the full-plane magnetoelectroelastic substrate.
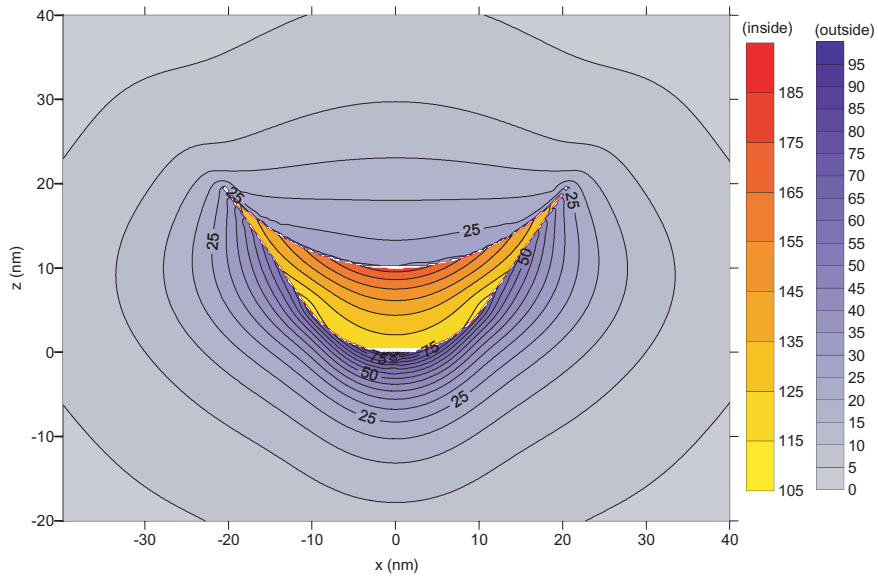
Fig. 13. Total electric field $\sqrt{E_x^2 + E_z^2}$ ($\times 10^7$ V/m) distribution inside and outside the crescent/V-shaped QWR in the full-plane magnetoelectroelastic substrate.
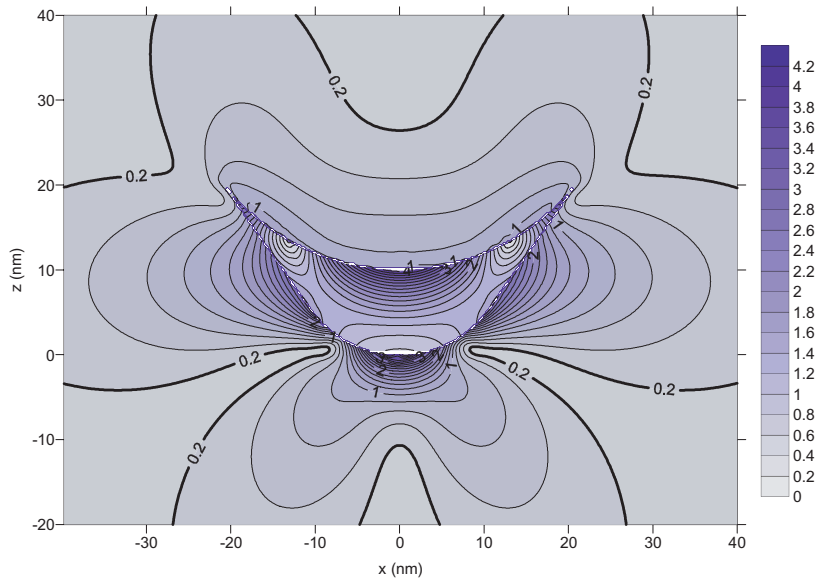

Fig. 14. Total magnetic field $\sqrt{H_x^2 + H_z^2}$ ($\times 10^7$ A/m) distribution inside and outside the crescent/V-shaped QWR in the full-plane magnetoelectroelastic substrate.

For the V-shaped QWR, the induced field shows the following characteristics:

(1) The induced field inside is much larger than that outside, with the exception of the magnetic field where both inside and outside fields have the same magnitude;

(2) With the exception of the magnetic field, the contours of the elastic strain and electric fields inside the QWR seem to follow the shape of the crescent curve;

(3) The electric field outside seems also to follow the shape of the crescent curve while the strain and magnetic fields outside show concentrations at different locations.

6. Conclusions

In this paper, we first derive the 2D line-source Green's functions in full-, half-, and bimaterial-planes of general anisotropic magnetoelectroelasticity. By virtue of the simple Green's function expression and the equivalent body-force concept, the elastic, electric, and magnetic fields due to an arbitrarily shaped inclusion with a uniform eigenstrain are derived in an exact closed form. The exact closed-form solution is then applied to the typical T- and V-shaped QWRs in full- and half-plane semiconductor substrates made of transversely isotropic magnetoelectroelastic materials. Numerical examples show various new features, which could be of interest in the future composite repair, and fabrication and design of novel semiconductor nanostructures made of anisotropic magnetoelectroelastic materials.

We also remark that the application of the exact closed-form solution to the QWR structure is based on the assumption that the QWR can be treated as an inclusion. In reality, the material property of the QWR, as a function of the mismatched lattice constants (Ellaway and Faux, 2002; Chung and Namburu, 2003), could be different from its surrounding matrix. The effect of the mismatched lattice constants on the QWR material property and the subsequent influence on the induced field is currently under investigation. Research results will be reported in the future.

Acknowledgements

Appendix A. Two-dimensional Green's functions for anisotropic magnetoelectroelastic bimaterials

Let us assume that materials 1 and 2 occupy, respectively, the half-planes $z > 0$ and $z < 0$. As in the text, we also assume that the deformation is in the (x, z)-plane and is independent of the y-coordinate. An extended line force $\boldsymbol{f} = (f_1, f_2, f_3, -f_e, -f_m)$ is applied at point (X, Z) in one of the half-planes. To derive the Green's functions, it is sufficient to find the extended displacement vector $\boldsymbol{u}$ and stress function vector $\boldsymbol{\psi}$ due to the extended line force (Ting, 1996; Pan, 2004a,b), which are presented below for different combinations of the source and field points.

Assume that the source point (X, Z) is in the half-plane of material λ ($\lambda = 1$ or 2). Then if the field point (x, z) is in the source plane (i.e., the half-plane of material λ), the displacement and stress function vectors can be expressed as

$$\boldsymbol{u}^{(\lambda)} = \frac{1}{\pi}\mathrm{Im}\left\{\boldsymbol{A}^{(\lambda)}\langle\ln(z_*^{(\lambda)} - s_*^{(\lambda)})\rangle\boldsymbol{q}^{\infty,\lambda}\right\} + \frac{1}{\pi}\mathrm{Im}\sum_{J=1}^{5}\left\{\boldsymbol{A}^{(\lambda)}\langle\ln(z_*^{(\lambda)} - \bar{s}_J^{(\lambda)})\rangle\boldsymbol{q}_J^{(\lambda)}\right\}$$

$$\boldsymbol{\psi}^{(\lambda)} = \frac{1}{\pi}\mathrm{Im}\left\{\boldsymbol{B}^{(\lambda)}\langle\ln(z_*^{(\lambda)} - s_*^{(\lambda)})\rangle\boldsymbol{q}^{\infty,\lambda}\right\} + \frac{1}{\pi}\mathrm{Im}\sum_{J=1}^{5}\left\{\boldsymbol{B}^{(\lambda)}\langle\ln(z_*^{(\lambda)} - \bar{s}_J^{(\lambda)})\rangle\boldsymbol{q}_J^{(\lambda)}\right\}$$

(A.1)

If the field point (x, z) is in the other half-plane of material $\mu (\mu \neq \lambda)$ ($\lambda, \mu = 1$ or 2), they have the form as

$$\boldsymbol{u}^{(\mu)} = \frac{1}{\pi} \operatorname{Im} \sum_{J=1}^{5} \left\{ \boldsymbol{A}^{(\mu)} \langle \ln(z_*^{(\mu)} - s_J^{(\lambda)}) \rangle \boldsymbol{q}_J^{(\mu)} \right\}$$

$$\boldsymbol{\psi}^{(\mu)} = \frac{1}{\pi} \operatorname{Im} \sum_{J=1}^{5} \left\{ \boldsymbol{B}^{(\mu)} \langle \ln(z_*^{(\mu)} - s_J^{(\lambda)}) \rangle \boldsymbol{q}_J^{(\mu)} \right\}$$

(A.2)

In Eqs. (A.1) and (A.2), the superscripts (λ) and (μ) denote the quantities associated with the material domains 1 and 2. $p_J^{(\lambda)}$, $\boldsymbol{A}^{(\lambda)}$, and $\boldsymbol{B}^{(\lambda)}$ are the Stroh eigenvalues and the corresponding eigenmatrices. Also in Eqs. (A.1) and (A.2), we have:

$$\langle \ln(z_*^{(\lambda)} - s_*^{(\lambda)}) \rangle = \operatorname{diag}[\ln(z_1^{(\lambda)} - s_1^{(\lambda)}),\ \ln(z_2^{(\lambda)} - s_2^{(\lambda)}),\ \ln(z_3^{(\lambda)} - s_3^{(\lambda)}),\ \ln(z_4^{(\lambda)} - s_4^{(\lambda)}),\ \ln(z_5^{(\lambda)} - s_5^{(\lambda)})]$$

$$\langle \ln(z_*^{(\lambda)} - \bar{s}_J^{(\lambda)}) \rangle = \operatorname{diag}[\ln(z_1^{(\lambda)} - \bar{s}_J^{(\lambda)}),\ \ln(z_2^{(\lambda)} - \bar{s}_J^{(\lambda)}),\ \ln(z_3^{(\lambda)} - \bar{s}_J^{(\lambda)}),\ \ln(z_4^{(\lambda)} - \bar{s}_J^{(\lambda)}),\ \ln(z_5^{(\lambda)} - \bar{s}_J^{(\lambda)})]$$

$$\langle \ln(z_*^{(\mu)} - s_J^{(\lambda)}) \rangle = \operatorname{diag}[\ln(z_1^{(\mu)} - s_J^{(\lambda)}),\ \ln(z_2^{(\mu)} - s_J^{(\lambda)}),\ \ln(z_3^{(\mu)} - s_J^{(\lambda)}),\ \ln(z_4^{(\mu)} - s_J^{(\lambda)}),\ \ln(z_5^{(\mu)} - s_J^{(\lambda)})]$$

(A.3)

where $z_J^{(\alpha)}$ and $s_J^{(\alpha)}$ ($\alpha = 1, 2$) are complex variables associated with the field and source points, respectively. They are defined as

$$z_J^{(\alpha)} = x + p_J^{(\alpha)} z, \quad s_J^{(\alpha)} = X + p_J^{(\alpha)} Z$$

(A.4)

We further observe that the first term in Eq. (A.1) corresponds to the full-plane Green's functions in material λ with

$$\boldsymbol{q}^{\infty,\lambda} = (\boldsymbol{A}^{(\lambda)})^{\mathrm{T}} \boldsymbol{f}$$

(A.5)

The second term in Eq. (A.1) and the term in Eq. (A.2) are the complementary parts of the Green's function solutions. Also the complex vectors $\boldsymbol{q}_J^{(\lambda)}$ ($\lambda = 1, 2$; $J = 1, 2, 3, 4, 5$) in Eq. (A.1) and $\boldsymbol{q}_J^{(\mu)}$ ($\mu = 1, 2$; $J = 1, 2, 3, 4, 5$) in Eq. (A.2) are determined using the continuity conditions along the interface of the two half-planes. After certain algebraic calculations, these vectors can be expressed as ($\lambda, \mu = 1$ or 2, but $\mu \neq \lambda$):

$$\boldsymbol{q}_J^{(\lambda)} = (\boldsymbol{A}^{(\lambda)})^{-1} (\boldsymbol{M}^{(\lambda)} + \bar{\boldsymbol{M}}^{(\mu)})^{-1} (\bar{\boldsymbol{M}}^{(\mu)} - \bar{\boldsymbol{M}}^{(\lambda)}) \bar{\boldsymbol{A}}^{(\lambda)} \boldsymbol{I}_J \bar{\boldsymbol{q}}^{\infty,\lambda}$$

(A.6a)

for Eq. (A.1); and

$$\boldsymbol{q}_J^{(\mu)} = (\boldsymbol{A}^{(\mu)})^{-1} (\bar{\boldsymbol{M}}^{(\lambda)} + \boldsymbol{M}^{(\mu)})^{-1} (\boldsymbol{M}^{(\lambda)} + \bar{\boldsymbol{M}}^{(\lambda)}) \boldsymbol{A}^{(\lambda)} \boldsymbol{I}_J \boldsymbol{q}^{\infty,\lambda}$$

(A.6b)

for Eq. (A.2). In Eqs. (A.6a) and (A.6b), matrix $M^{(\alpha)}$ is the impedance tensor defined as

$$\boldsymbol{M}^{(\alpha)} = -i\boldsymbol{B}^{(\alpha)} (\boldsymbol{A}^{(\alpha)})^{-1} \quad (\alpha = 1, 2)$$

(A.7)

and the diagonal matrix $\boldsymbol{I}_J$ has the following expression for different indexes J:

$$\boldsymbol{I}_1 = \operatorname{diag}[1, 0, 0, 0, 0]; \quad \boldsymbol{I}_2 = \operatorname{diag}[0, 1, 0, 0, 0]; \quad \boldsymbol{I}_3 = \operatorname{diag}[0, 0, 1, 0, 0];$$

$$\boldsymbol{I}_4 = \operatorname{diag}[0, 0, 0, 1, 0]; \quad \boldsymbol{I}_5 = \operatorname{diag}[0, 0, 0, 0, 1]$$

(A.8)

Appendix B. Analytical solution for arbitrarily shaped polygonal inclusion in anisotropic magnetoelectroelastic bimaterials

Following the same procedure in Pan (2004a,b) and assuming that the inclusion with general coordinate $\boldsymbol{x} = (x, z)$ (i.e., the field point of the line-source Green's functions) is in the half-plane of material

$\lambda(\lambda = 1$ or $2)$, we derive the exact closed-form solution for the induced extended displacement vector due to the contribution of a straight-line segment of the boundary of the inclusion. That is, when the field point $X = (X, Z)$ (i.e., the source point in the line-source Green's functions) is in material λ, we have

$$u_K(X) = n_i C_{iJLm}^{(\lambda)} \gamma_{Lm}^* \frac{l}{\pi} \text{Im}\left\{ A_{JR}^{(\lambda)} h_R^{(\lambda)}(X, Z) A_{KR}^{(\lambda)} + \sum_{v=1}^{5} A_{JR}^{(\lambda)} w_{Rv}^{(\lambda)}(X, Z) Q_{RK}^{\lambda\lambda, v} \right\} \tag{B.1}$$

and when the field point X is in material $\mu(\mu = 1$ or 2, but $\mu \neq \lambda)$ the solution is

$$u_K(X) = n_i C_{iJLm}^{(\lambda)} \gamma_{Lm}^* \frac{l}{\pi} \text{Im}\left\{ \sum_{v=1}^{5} A_{JR}^{(\lambda)} g_{Rv}^{\lambda\mu}(X, Z) Q_{RK}^{\mu\lambda, v} \right\} \tag{B.2}$$

where n_i is the ith outward normal component; l is the length of the line segment over the boundary of the polygon, which can be expressed as $l = \sqrt{(x_2 - x_1)^2 + (z_2 - z_1)^2}$ by setting the generic line segment from point 1 (x_1, z_1) to point 2 (x_2, z_2). Consequently, the outward normal components n_i are constants, given by

$$n_1 = (z_2 - z_1)/l; \quad n_3 = -(x_2 - x_1)/l \tag{B.3}$$

In Eq. (B.1), A is the eigenmatrix corresponding to the Stroh eigenvalues p_J discussed in Appendix A, and the matrix Q is defined as $(\lambda, \mu = 1$ or 2, but $\lambda \neq \mu)$:

$$Q_{RN}^{\lambda\lambda, v} = K_{RP}^{\lambda\lambda}(I_v)_P \bar{A}_{NP}^{(\lambda)}$$
$$Q_{RN}^{\lambda\mu, v} = K_{RP}^{\lambda\mu}(I_v)_P A_{NP}^{(\lambda)} \tag{B.4}$$

where the matrix K is given by

$$K^{\lambda\lambda} = \left(A^{(\lambda)}\right)^{-1} \left(M^{(\lambda)} + \bar{M}^{(\mu)}\right)^{-1} \left(\bar{M}^{(\mu)} - \bar{M}^{(\lambda)}\right) \bar{A}^{(\lambda)}$$
$$K^{\lambda\mu} = \left(A^{(\mu)}\right)^{-1} \left(M^{(\mu)} + \bar{M}^{(\lambda)}\right)^{-1} \left(M^{(\lambda)} + \bar{M}^{(\lambda)}\right) A^{(\lambda)} \tag{B.5}$$

Also in Eq. (B.1), the term containing $h_R^{(\lambda)}$ stands for the contribution from the full-plane Green's function, and those involving $w_{Rv}^{(\lambda)}$ in (B.1) and $g_{Rv}^{\lambda\mu}$ in (B.2) for the contribution from the interface condition of the bimaterials. These functions are defined as

$$h_R^{(\lambda)}(X, Z) \equiv \int_0^1 \ln(z_R^{(\lambda)} - s_R^{(\lambda)}) \, dt$$
$$g_{Rv}^{\lambda\mu}(X, Z) \equiv \int_0^1 \ln(z_R^{(\lambda)} - s_v^{(\mu)}) \, dt \tag{B.6}$$
$$w_{Rv}^{(\lambda)}(X, Z) \equiv \int_0^1 \ln(z_R^{(\lambda)} - \bar{s}_v^{(\lambda)}) \, dt$$

and eventually have explicit expressions as

$$h_R^{(\lambda)}(X, Z) = \frac{(x_1 + p_R^{(\lambda)} z_1) - s_R^{(\lambda)}}{(x_2 - x_1) + p_R^{(\lambda)}(z_2 - z_1)} \ln\left[\frac{x_2 + p_R^{(\lambda)} z_2 - s_R^{(\lambda)}}{x_1 + p_R^{(\lambda)} z_1 - s_R^{(\lambda)}}\right] + \ln[x_2 + p_R^{(\lambda)} z_2 - s_R^{(\lambda)}] - 1$$

$$g_{Rv}^{\lambda\mu}(X, Z) = \frac{(x_1 + p_R^{(\lambda)} z_1) - s_v^{(\mu)}}{(x_2 - x_1) + p_R^{(\lambda)}(z_2 - z_1)} \ln\left[\frac{x_2 + p_R^{(\lambda)} z_2 - s_v^{(\mu)}}{x_1 + p_R^{(\lambda)} z_1 - s_v^{(\mu)}}\right] + \ln[x_2 + p_R^{(\lambda)} z_2 - s_v^{(\mu)}] - 1 \tag{B.7}$$

$$w_{Rv}^{(\lambda)}(X, Z) = \frac{(x_1 + p_R^{(\lambda)} z_1) - \bar{s}_v^{(\lambda)}}{(x_2 - x_1) + p_R^{(\lambda)}(z_2 - z_1)} \ln\left[\frac{x_2 + p_R^{(\lambda)} z_2 - \bar{s}_v^{(\lambda)}}{x_1 + p_R^{(\lambda)} z_1 - \bar{s}_v^{(\lambda)}}\right] + \ln[x_2 + p_R^{(\lambda)} z_2 - \bar{s}_v^{(\lambda)}] - 1$$

Using the strain/displacement, electric field/electric potential, and magnetic field/magnetic potential relations, the elastic strain, electric, and magnetic fields can be obtained in the exact closed form. Assuming that the inclusion is in the inclusion half-plane of material λ ($\lambda = 1$ or 2), we find the contribution of the straight-line segment of the polygon to the strain, electric, and magnetic fields as follows. When the field point X is in the half-plane of material λ, we have ($\alpha, \beta = 1, 3$):

$$\gamma_{\beta\alpha}(\boldsymbol{X}) = 0.5 n_i C_{iJLm}^{(\lambda)} \gamma_{Lm}^* \frac{l}{\pi} \mathrm{Im} \left\{ A_{JR}^{(\lambda)} h_{R,\alpha}^{(\lambda)}(X,Z) A_{\beta R}^{(\lambda)} + \sum_{v=1}^{5} A_{JR}^{(\lambda)} w_{Rv,\alpha}^{(\lambda)}(X,Z) Q_{R\beta}^{\lambda\lambda,v} \right\}$$

$$+ 0.5 n_i C_{iJLm}^{(\lambda)} \gamma_{Lm}^* \frac{l}{\pi} \mathrm{Im} \left\{ A_{JR}^{(\lambda)} h_{R,\beta}^{(\lambda)}(X,Z) A_{\alpha R}^{(\lambda)} + \sum_{v=1}^{5} A_{JR}^{(\lambda)} w_{Rv,\beta}^{(\lambda)}(X,Z) Q_{R\alpha}^{\lambda\lambda,v} \right\}$$

$$\gamma_{2\alpha}(\boldsymbol{X}) = 0.5 n_i C_{iJLm}^{(\lambda)} \gamma_{Lm}^* \frac{l}{\pi} \mathrm{Im} \left\{ A_{JR}^{(\lambda)} h_{R,\alpha}^{(\lambda)}(X,Z) A_{2R}^{(\lambda)} + \sum_{v=1}^{5} A_{JR}^{(\lambda)} w_{Rv,\alpha}^{(\lambda)}(X,Z) Q_{R2}^{\lambda\lambda,v} \right\} \qquad \text{(B.8)}$$

$$E_{\alpha}(\boldsymbol{X}) = -n_i C_{iJLm}^{(\lambda)} \gamma_{Lm}^* \frac{l}{\pi} \mathrm{Im} \left\{ A_{JR}^{(\lambda)} h_{R,\alpha}^{(\lambda)}(X,Z) A_{4R}^{(\lambda)} + \sum_{v=1}^{5} A_{JR}^{(\lambda)} w_{Rv,\alpha}^{(\lambda)}(X,Z) Q_{R4}^{\lambda\lambda,v} \right\}$$

$$H_{\alpha}(\boldsymbol{X}) = -n_i C_{iJLm}^{(\lambda)} \gamma_{Lm}^* \frac{l}{\pi} \mathrm{Im} \left\{ A_{JR}^{(\lambda)} h_{R,\alpha}^{(\lambda)}(X,Z) A_{5R}^{(\lambda)} + \sum_{v=1}^{5} A_{JR}^{(\lambda)} w_{Rv,\alpha}^{(\lambda)}(X,Z) Q_{R5}^{\lambda\lambda,v} \right\}$$

and when field point is in the other half-plane of material μ ($\lambda, \mu = 1$ or 2, but $\mu \neq \lambda$), the induced fields are

$$\gamma_{\beta\alpha}(\boldsymbol{X}) = 0.5 n_i C_{iJLm}^{(\lambda)} \gamma_{Lm}^* \frac{l}{\pi} \mathrm{Im} \left\{ \sum_{v=1}^{5} A_{JR}^{(\lambda)} g_{Rv,\alpha}^{\lambda\mu}(X,Z) Q_{R\beta}^{\mu\lambda,v} + \sum_{v=1}^{5} A_{JR}^{(\lambda)} g_{Rv,\beta}^{\lambda\mu}(X,Z) Q_{R\alpha}^{\mu\lambda,v} \right\}$$

$$\gamma_{2\alpha}(\boldsymbol{X}) = 0.5 n_i C_{iJLm}^{(\lambda)} \gamma_{Lm}^* \frac{l}{\pi} \mathrm{Im} \left\{ \sum_{v=1}^{5} A_{JR}^{(\lambda)} g_{Rv,\alpha}^{\lambda\mu}(X,Z) Q_{R2}^{\mu\lambda,v} \right\}$$

$$E_{\alpha}(\boldsymbol{X}) = -n_i C_{iJLm}^{(\lambda)} \gamma_{Lm}^* \frac{l}{\pi} \mathrm{Im} \left\{ \sum_{nu=1}^{5} A_{JR}^{(\lambda)} g_{Rv,\alpha}^{\lambda\mu}(X,Z) Q_{R4}^{\mu\lambda,v} \right\} \qquad \text{(B.9)}$$

$$H_{\alpha}(\boldsymbol{X}) = -n_i C_{iJLm}^{(\lambda)} \gamma_{Lm}^* \frac{l}{\pi} \mathrm{Im} \left\{ \sum_{v=1}^{5} A_{JR}^{(\lambda)} g_{Rv,\alpha}^{\lambda\mu}(X,Z) Q_{R5}^{\mu\lambda,v} \right\}$$

References

Aboudi, J., 2000. Micromechanical prediction of the effective behavior of fully coupled electro-magneto-thermo-elastic multiphase composites. NASA/CR2000-209787, pp. 1–16.

Aboudi, J., 2001. Micromechanical analysis of fully coupled electro-magneto-thermo-elastic multiphase composites. Smart Mater. Struct. 10, 867–877.

Andreev, A.D., O'Reilly, E.P., 2000. Theory of the electronic structure of GaN/AlN hexagonal quantum dots. Phys. Rev. B 62, 15851–15870.

Austing, D.G., Sasaki, S., Tarucha, S., Reimann, S.M., Koskinen, M., Manninen, M., 1999. Ellipsoidal deformation of vertical quantum dots. Phys. Rev. B 60, 11514–11523.

Benveniste, Y., 1995. Magnetoelectric effect in fibrous composites with piezoelectric and piezomagnetic phases. Phys. Rev. B 51, 16424–16427.

Caro, L.D., Tapfer, L., 1995. Strain and piezoelectric fields in arbitrarily oriented semiconductor heterostructures. II. Quantum wires. Phys. Rev. B 51, 4381–4387.

Chen, W.Q., Lee, K.Y., 2003. Alternative state space formulations for magnetoelectric thermoelasticity with transverse isotropy and the application to bending analysis of nonhomogeneous plates. Int. J. Solids Struct. 40, 5689–5705.

Chung, P.W., Namburu, R.R., 2003. On a formulation for a multiscale atomistic-continuum homogenization method. Int. J. Solids Struct. 40, 2563–2588.

Daher, N., 1996. Electromagnetomechanical media including irreversible processes and interfacial properties. Synth. Met. 76, 327–330.

Dietl, T., Ohno, H., Matsukura, F., 2001. Hole-mediated ferromagnetism in tetrahedrally coordinated semiconductors. Phys. Rev. B 63, 195–205.

Ding, H.J., Jiang, A.M., 2003. Fundamental solutions for transversely isotropic magneto-electro-elastic media and boundary integral formulation. Sci. China E 46, 607–619.

Duong, C.N., Yu, J., 2003. Analysis of a plate containing a polygon-shaped inclusion with a uniform eigencurvature. J. Appl. Mech. 70, 404–407.

Ellaway, S.W., Faux, D.A., 2002. Effective elastic stiffness of InAs under uniform strain. J. Appl. Phys. 92, 3027–3033.

Erber, T., Guralnick, S.A., Desai, R.D., Kwok, W., 1997. Piezomagnetism and fatigue. J. Phys. D: Appl. Phys. 30, 2818–2836.

Eshelby, J.D., 1957. The determination of the elastic field of an ellipsoidal inclusion and related problem. Proc. Roy. Soc. A 241, 376–396.

Faux, D.A., Downes, J.R., O'Reilly, E.P., 1997. Analytic solutions for strain distribution in quantum-wire structures. J. Appl. Phys. 82, 3754–3762.

Fiebig, M., Lottermoser, Th., Frohlich, D., Goltsev, A.V., Pisarev, R.V., 2002. Observation of coupled magnetic and electric domains. Nature 419, 818–820.

Frank, T., Schilling, C., 1998. The development of cascadable microdrives with muscle-like operating behaviour. J. Micromech. Microeng. 8, 222–229.

Gao, C.-F., Kessler, H., Balke, H., 2003a. Crack problems in magnetoelectroelastic solids. Part I: exact solution of a crack. Int. J. Engng. Sci. 41, 969–981.

Gao, C.-F., Tong, P., Zhang, T.Y., 2003b. Interfacial crack problems in magneto-electroelastic solids. Int. J. Engng. Sci. 41, 2105–2121.

Gibbs, M.R.J., Watts, R., Karl, W., Powell, A.L., Yates, R.B., 1997. Microstructures containing piezomagnetic elements. Sensors Actuat. A 59, 229–235.

Gippius, N.A., Tikhodeev, S.G., Forchel, A., Kulakovskii, V.D., 1994. Polarization-dependent optical effects in open quantum well wires. Superlatt. Microstruct. 16, 165–167.

Glas, F., 2003. Elastic relaxation of a truncated circular cylinder with uniform dilatational eigenstrain in a half space. Phys. Stat. Sol. B 237, 599–610.

Goldoni, G., Rossi, F., Molinari, E., Fasolino, A., Rinaldi, R., Cingolani, R., 1996. Valence band spectroscopy in V-grooved quantum wires. Appl. Phys. Lett. 69, 2965–2967.

Goldoni, G., Rossi, F., Molinari, E., 1997a. Excitonic effects in quantum wires. Phys. Stat. Sol. (a) 164, 265–271.

Goldoni, G., Rossi, F., Molinari, E., 1997b. Quantum interference in nanometric devices: Ballistic transport across array of T-shaped quantum wires. Appl. Phys. Lett. 71, 1519–1521.

Goldoni, G., Rossi, F., Molinari, E., 1999. Strong exciton binding in hybrid GaAs-based nanostructures. Physica B 272, 518–521.

Grundmann, M., Stier, O., Bimberg, D., 1994. Symmetry breaking in pseudomorphic V-groove quantum wires. Phys. Rev. B 50, 14187–14192.

Grundmann, M., Stier, O., Bimberg, D., 1998. Electronic states in strained cleaved-edge-overgrowth quantum wires and quantum dots. Phys. Rev. B 58, 10557–10561.

Gustafsson, A., Samuelson, L., Hessman, D., Malm, J.-O., Vermeire, G., Demeester, P., 1994. Characterization of a single-layer quantum wire structure grown directly on a submicron grating. J. Vac. Sci. Technol. B 13, 308–317.

Gustafsson, A., Malm, J.-O., Carlsson, A., Vermeire, G., 1996. High-resolution transmission electron microscopy studies of quantum wire structures grown on submicrometre gratings of V-grooves. Semicond. Sci. Technol. 11, 1745–1755.

Horiguchi, K., Shindo, Y., 2003. Experimental and theoretical results for bending of a soft ferromagnetic plate in a transversely magnetic field. Acta Mech. 162, 185–194.

Huang, J.H., Kuo, W.-S., 1997. The analysis of piezoelectric/peizomagnetic composite materials containing ellipsoidal inclusions. J. Appl. Phys. 81, 1378–1386.

Itoh, H., Hayamizu, Y., Yoshita, M., Akiyama, H., Pfeiffer, L.N., West, K.W., Szymanska, M.H., Littlewood, P.B., 2003. Polarization-dependent photoluminescence-excitation spectra of one-dimensional exciton and continuum states in T-shaped quantum wires. Appl. Phys. Lett. 83, 2043–2045.

Jogai, B., Albrecht, J.D., Pan, E., 2003. Electromechanical coupling in free-standing AlGaN/GaN planar structures. J. Appl. Phys. 94, 6566–6573.

Kapon, E., Hwang, D.M., Bhat, R., 1989. Stimulated emission in semiconductor quantum wire heterostructures. Phys. Rev. Lett. 63, 430–433.

Kapon, E., Walther, M., Christen, J., Grundmann, M., Caneau, C., Hwang, D.M., Colas, E., Bhat, R., Song, G.H., Bimberg, D., 1992. Quantum wire heterostructures for optoelectronic applications. Superlatt. Microstruct. 12, 491–499.

Lang, I.G., Korovin, L.I., Cruz-Alcaz, J.A. de la, Pavlov, S.T., 2003. Quantum theory of conductivity of spatially inhomogeneous systems. J. Exp. Theor. Phys. 96, 268–285.

Li, J.Y., 2000. Magnetoelectroelastic multi-inclusion and inhomogeneity problems and their applications in composite materials. Int. J. Engng. Sci. 38, 1993–2011.

Li, J.Y., 2003. Uniqueness and reciprocity theorems for linear thermo-electro-magneto-elasticity. Q. J. Mech. Appl. Math. 56, 35–43.

Li, J.Y., Dunn, M.L., 1998. Anisotropic coupled-field inclusion and inhomogeneity problems. Philos. Mag. A 77, 1341–1350.

Liu, J.-X., Liu, X.-L., Zhao, Y.-B., 2001. Green's functions for anisotropic magnetoelectroelastic solids with an elliptical cavity or a crack. Int. J. Engng. Sci. 39, 1405–1418.

Liu, X.-Q., Wang, X.-L., Ogura, M., Guillet, T., Voliotis, V., Grousson, R., 2002. Piezoelectric effects in ultrahigh quality AlGaAs/GaAs single quantum wire. Physica E 13, 194–198.

Lomascolo, M., Rinaldi, R., Passaseo, A., Vittorio, M.D., Giorgi, M.D., Cingolani, R., Caro, L.D., Tapfer, L., Taurino, A., Catalano, M., 1999. Time resolved screening of the piezoelectric field in InGaAs/GaAs V-shaped quantum wires of variable profile. J. Phys.: Condens. Matter. 11, 5989–5997.

Lomascolo, M., Anni, M., Giorgi, M.D., Rinaldi, R., Passaseo, A., Cingolani, R., Lorenzoni, A., Andreani, L.C., 2000. Time-resolved magnetospectroscopy of $In_xGa_{1-x}As$/GaAs V-shaped quantum wires. Phys. Rev. B 61, 12658–12661.

Mauritz, O., Goldoni, G., Molinari, E., Rossi, F., 2000. Local optical spectroscopy of semiconductor nanostructures in the linear regime. Phys. Rev. B 62, 8204–8211.

Mazumder, S., Battacharyya, G.S., 2003. Magnetoelectric behavior in in situ grown piezoelectric and piezomagnetic composite-phase system. Mater. Res. Bull. 38, 303–310.

Meeker, D.C., Dozor, D.M., 1999. Thermomagnetic optimization of solenoidal magnetostrictive actuators. In: Smart Structures and Materials. Newport Beach, CA, March, 1999.

Miura, N., Kunimastsu, H., Uchida, K., Matsuda, Y., Yasuhira, T., Nakashima, H., Sakuma, Y., Awano, Y., Futatsugi, T., Yokoyama, N., 1998. Magneto-optical study of excitons in quantum wells, wires and dots in high magnetic fields. Physica B 256–258, 308–318.

Mura, T., 1987. Micromechanics of Defects in Solids, second ed. Kluwer Academic Publishers.

Mura, T., 1997. The determination of the elastic field of a polygonal star shaped inclusion. Mech. Res. Commun. 24, 473–482.

Nan, C.-W., 1994. Magnetoelectric effect in composites of piezoelectric and piezomagnetic phases. Phys. Rev. B 50, 6082–6088.

Nozaki, H., Taya, M., 1997. Elastic fields in a polygon-shaped inclusion with uniform eigenstrains. J. Appl. Mech. 64, 495–502.

Pan, E., 2001. Exact solution for simply supported and multilayered magneto-electro-elastic plates. J. Appl. Mech. 68, 608–618.

Pan, E., 2002a. Three-dimensional Green's functions in anisotropic magneto-electro-elastic bimaterials. Z. Angew. Math. Phys. 53, 815–838.

Pan, E., 2002b. Elastic and piezoelectric fields around a quantum dot: Fully coupled or semicoupled model? J. Appl. Phys. 91, 3785–3796.

Pan, E., 2004a. Eshelby Problem of polygonal inclusion in anisotropic piezoelectric full- and half-planes. J. Mech. Phys. Solids 52, 567–589.

Pan, E., 2004b. Eshelby Problem of polygonal inclusions in anisotropic piezoelectric bimaterials. Proceedings of the Royal Society of London A 460, 537–560.

Pan, E., Han, F. Exact solution for functionally graded and layered magneto-electro-elastic plates, submitted for publication.

Pan, E., Heyliger, P.R., 2002. Free vibrations of simply supported and multilayered magneto-electro-elastic plates. J. Sound Vibrat. 252, 429–442.

Pan, E., Jiang, X., 2003. QWR induced elastic strain and electric field on the surface of semiconductor substrate GaAs. In: Proceedings of the 2003 International Conference on Computational & Experimental Engineering & Sciences, Corfu, Greece, 2003.

Park, Y.D., Hanbicki, A.T., Erwin, S.C., Hellberg, C.S., Sullivan, J.M., Mattson, J.E., Ambrose, T.F., Wilson, A., Spanos, G., Jonker, B.T., 2002. A group-IV ferromagnetic semiconductor: Mn_xGe_{1-x}. Science 295, 651–654.

Rinaldi, R., Cingolani, R., Lepore, M., Ferrara, M., Catalano, I.M., Rossi, F., Rota, L., Molinari, E., Lugli, P., Marti, U., Martin, D., Morier-Gemoud, F., Ruterana, P., Reinhart, F.K., 1994. Exciton binding energy in GaAs V-shaped quantum wires. Phys. Rev. Lett. 73, 2899–2902.

Rodin, G.J., 1996. Eshelby's inclusion problem for polygons and polyhedra. J. Mech. Phys. Solids 44, 1977–1995.

Rossi, F., Goldoni, G., Molinari, E., 1997. Shape-independent scaling of excitonic confinement in realistic quantum wires. Phys. Rev. Lett. 78, 3527–3530.

Rossi, F., Goldoni, G., Mauritz, O., Molinari, E., 1999. Theory of excitonic confinement in semiconductor quantum wires. J. Phys.: Condens. Matter. 11, 5969–5988.

Ru, C.Q., 1999. Analytical solution for Eshelby's problem of an inclusion of arbitrary shape in a plane or half-plane. J. Appl. Mech. 66, 315–322.

Ru, C.Q., 2000. Eshelby's problem for two-dimensional piezoelectric inclusions of arbitrary shape. Proc. R. Soc. Lond. A. 456, 1051–1068.

Ryu, J., Priya, S., Uchino, K., Kim, H.-E., 2002. Magnetoelectric effect in composites of magnetostrictive and piezoelectric materials. J. Electroceram. 8, 107–119.

Sander, D., 1999. The correlation between mechanical stress and magnetic anisotropy in ultrathin films. Rep. Prog. Phys. 62, 809–858.

Soh, A.K., Liu, J.X., Hoon, K.H., 2003. Three-dimensional Green's functions for transversely isotropic magnetoelectroelastic solids. Int. J. Nonlinear Sci. 4, 139–148.

Ting, T.C.T., 1996. Anisotropic Elasticity. Oxford University Press, Oxford.

Wang, X., Shen, Y.-P., 2003. Inclusions of arbitrary shape in magnetoelectroelastic composite materials. Int. J. Engng. Sci. 41, 85–102.

Wang, X., Zhong, Z., 2003a. A circular tube or bar of cylindrically anisotropic magnetoelectroelastic material under pressuring loading. Int. J. Engng. Sci. 41, 2143–2159.

Wang, X., Zhong, Z., 2003b. Three-dimensional solution of smart laminated anisotropic circular cylindrical shells with imperfect bonding. Int. J. Solids Struct. 40, 5901–5921.

Yu, H.Y., 2001. Two-dimensional elastic defects in orthotropic bicrystals. J. Mech. Phys. Solids 49, 261–287.